



ELSEVIER

Available online at [www.sciencedirect.com](http://www.sciencedirect.com)

SCIENCE @ DIRECT®

Journal of Organometallic Chemistry 678 (2003) 156–165

Journal  
of Organo  
metallic  
Chemistry[www.elsevier.com/locate/jorganchem](http://www.elsevier.com/locate/jorganchem)

# A study on the excitations of ligand-to-metal charge transfer in complexes $\text{Cp}_2\text{MCl}_2$ ( $\text{Cp} = \pi\text{-C}_5\text{H}_5$ , $\text{M} = \text{Ti}, \text{Zr}, \text{Hf}$ ) by density functional theory

Xiaojing Wang<sup>a</sup>, Lv Chen<sup>a</sup>, Akira Endou<sup>a</sup>, Momoji Kubo<sup>a</sup>, Akira Miyamoto<sup>a,b,\*</sup><sup>a</sup> Department of Materials Chemistry, Graduate School of Engineering, Tohoku University, Aoba-yama 07, Sendai 980-8579, Japan<sup>b</sup> New Industry Creation Hatchery Center (NICHe), Tohoku University, Aoba-yama 04, Sendai 980-8579, Japan

Received 7 February 2003; received in revised form 13 May 2003; accepted 13 May 2003

## Abstract

The excitations of ligand-to-metal charge transfer in the UV–vis spectra of the complexes  $\text{Cp}_2\text{MCl}_2$  ( $\text{Cp} = \pi\text{-C}_5\text{H}_5$ ,  $\text{M} = \text{Ti}, \text{Zr}, \text{Hf}$ ) were described with the time-dependent density functional theory and the differential self-consistent-field density functional theory ( $\Delta\text{SCF-DFT}$ ). The nature of the main spectral features was interpreted on the basis of the electronic structure of the complexes. The optimization of the molecular structure for  $\text{Cp}_2\text{MCl}_2$  yielded consistent pseudotetrahedral geometries. With the transition from ground state to excited state, the electrons transferred from Cp ligands to the central metals M, accompanied by an increase in the binding length of M–Cl. This transfer process accounted for the first two absorption bands observed experimentally. The energies and oscillator strengths for the low-lying excitations depended strongly on the nature of the central metals. With varying the central metals from Ti, Zr, and to Hf, the energy gap increased between the sets of highest occupied molecular orbitals (HOMOs) and the sets of lowest unoccupied molecular orbitals (LUMOs). This increase was originated from an increment of energy for the LUMO sets that are mainly of d orbital of the metal and a relatively stable energy level of the HOMO sets that are mainly of p-orbital of Cp and Cl ligands. The excitation energies calculated by these methods showed a small difference, which can be well understood by a relativistic effect. The predicted level patterns of the lowest triplet excited states fit well the available phosphorescence data.

© 2003 Elsevier B.V. All rights reserved.

**Keywords:** Ligand-to-metal charge transfer; Excited state; Electronic spectrum; Organometallic complexes; Density functional theory

## 1. Introduction

The researches on photophysics and photochemistry of organometallic complexes have received intensive attention due to the great applications of these complexes in many fields such as photocatalysis, optical reaction, material design, and solar energy conversion [1–5]. One of the most intriguing spectroscopic characteristics for the organometallic complexes is that an intramolecular electron transfer may take place during

the excitations [6–9]. It is known to originate from the electronic transitions between various types of orbitals that are usually  $\pi$ -bonding orbitals in ligands or d orbitals in transition metals.  $\text{Cp}_2\text{MCl}_2$  ( $\text{Cp} = \pi\text{-C}_5\text{H}_5$ ,  $\text{M} = \text{Ti}, \text{Zr}, \text{Hf}$ ) is a series of model complexes for an understanding of the electronic transfer between these orbitals, because they have similar geometry structure [10–12], and any change in the optical properties can clearly give some information about the mechanisms of the electronic transfer. Furthermore, for  $\text{Cp}_2\text{MCl}_2$  ( $\text{M} = \text{Ti}, \text{Zr}, \text{Hf}$ ), the excitations assigned to the ligand-to-metal charge transfer (LMCT) occur mainly in the visible optical region [13–15], which is completely different from most organometallic complexes [16,17]. For the latter cases, the electronic transfer from ligands

\* Corresponding author. Tel.: +81-22-217-7233; fax: +81-22-217-7235.

E-mail address: [miyamoto@aki.che.tohoku.ac.jp](mailto:miyamoto@aki.che.tohoku.ac.jp) (A. Miyamoto).

to central metals usually appears at higher energies and overlaps with numerous electronic transfers from metals-to-ligands, which makes it very difficult to do spectroscopic assignments by experiments or theoretical simulations.

An analysis of the electronic luminescence spectra of both  $\text{Cp}_2\text{Zr}(\text{SR})_2$  and  $\text{Cp}_2\text{Hf}(\text{SR})_2$  indicates that the lowest transitions are assigned to the predominant LMCT admixed with a ligand-to-ligand charge transfer [18], however, their excitation energies and oscillator strengths of LMCT are different [19]. Loukova and Smirnov [20] studied the luminescence of  $\text{Cp}_2\text{MCl}_2$  ( $\text{M} = \text{Ti}, \text{Zr}, \text{Hf}$ ) in glassy solutions and solid state, and found that upon photoexcitation, the titanocene gives a red luminescence, while the zirconocene and hafnocene exhibit strong blue/green luminescence. On the other hand, the spectra for titanocene are sharp and narrow, while the zirconocene emission profiles are broad and slightly structured. The emission patterns for hafnocene are also similar to those for zirconocene with the exception that the emission maximum and the 0–0 transition band edges appear at higher energies [20]. The photophysical dynamics of the LMCT relaxation process is therefore determined by the nature of the metal–ligand binding. The relative energies and patterns of the excitations could be controlled by changing the ligands or the central metals. However, there are still some ambiguities relating to the electronic transfer, e.g. whether the lowest LMCT excitations of the complex  $\text{Cp}_2\text{MCl}_2$  are primarily due to the charge transfer of  $\text{Cl} \rightarrow \text{M}$  or  $\text{Cp} \rightarrow \text{M}$ , and what is the fraction of charge that transferred from the central metals to the ligands.

A comprehensive understanding of the spectral properties by systematic analyses of the electronic structure and the binding nature appear to be very important in solving the above ambiguities. Accurate quantum chemistry calculations can give reasonable characterization of the properties associated with the excited states and ground state, and furthermore can make detailed spectroscopic assignments. Several theoretical results have been reported concerning the electronic structures of the complexes  $\text{Cp}_2\text{MCl}_2$  [21–23], however most of which are concentrated on the properties relating to the ground states. In fact, the optical properties are closely related to the corresponding excited states, however, such theoretical work is still bare owing to the great difficulty in computation [24]. The few available studies of the optical properties do not give reasonable spectroscopic assignments or mechanism explanation for the transitions [25,26].

In this work, we reported on a theoretical investigation of the properties relating to both ground states and excited states for the complexes  $\text{Cp}_2\text{MCl}_2$  ( $\text{Cp} = \pi\text{-C}_5\text{H}_5$ ,  $\text{M} = \text{Ti}, \text{Zr}, \text{Hf}$ ) with an aim to well understand their intrinsic relationships among electronic structure and spectroscopic properties, and furthermore to reveal the

nature of excitations associated with the charge transfer between ligands and central metals. We also provided a detailed analysis of the absorption and phosphorescence spectroscopy, and explained the effects of different central metals on the charge transfer during the excitations by density functional theory calculations.

## 2. Method and computational details

In this study, the electronic structure and spectroscopic properties of the complexes  $\text{Cp}_2\text{MCl}_2$  ( $\text{Cp} = \pi\text{-C}_5\text{H}_5$ ,  $\text{M} = \text{Ti}, \text{Zr}, \text{Hf}$ ) were calculated by density functional theory using GAUSSIAN-98 (G98) [27] and Amsterdam Density Function (ADF1999) [28] program package, respectively. Total energies ( $E$ ) were calculated in term of the equation of  $E = E_T + E_V + E_J + E_{XC}$ , where  $E_T$  represents the kinetic energy term that arises from the motion of the electrons,  $E_V$  denotes the potential energies of nuclear-electron attraction and of the repulsion between pairs of nuclei,  $E_J$  is the electron–electron repulsion term that is also taken as the coulomb self-interaction of the electron density, and  $E_{XC}$  corresponds to the exchange and correlation term as well as the remaining part of the electron–electron interactions. All terms except the nuclear–nuclear repulsion are functions of the electron density  $\rho$ . In the case of G98, a mixture of Hartree-Fock and DFT along with a Becke three-parameter hybrid functional of Lee, Yang and Parr (B3LYP) was used as the exchange and correlation functional [29]. A standard LANL2DZ basis set was applied to all atoms [30]. In the case of ADF, the Perdew and Wang's 1991 exchange and correlation functional (PW91XC) was used in the generalized gradient approximation (GGA) [31], and triple- $\xi$  STO was applied to the valence electrons of all atoms. The shells (up to 2p for Ti, 3d for Zr and 4d for Hf) were treated as frozen cores. The relativistic terms were calibrated by a combined scalar relativistic zero order regular approximation (ZORA) [32]. The excitation energies and oscillator strengths of low-lying singlet and triplet excitation states of these complexes were derived by the method of time-dependent density functional theory (TDDFT) within the adiabatic approximation [33,34]. In order to get the geometry structure and electronic properties of excited states, the first excited states were calculated by differential self-consistent-field density functional theory ( $\Delta\text{SCF-DFT}$ ), in which the separate self-consistent-field calculations were performed to optimize the ground state and the appropriate excited state determinants [35]. The picture of the molecular orbital and optimized structure was illustrated using a MOLEKEL4.1 molecular visualization program [36].

### 3. Results and discussion

#### 3.1. Electronic structure and properties at ground state and excited state

The molecular structures of  $\text{Cp}_2\text{TiCl}_2$  and  $\text{Cp}_2\text{ZrCl}_2$  have been determined by electron diffraction in the vapor phase, they are a wedge-like sandwich structures with non-parallel rings, and exhibit a distorted tetrahedral arrangement of the  $\pi$ -cyclopentadienyl and chloride ligands in an idealized  $C_2$  symmetry [11,12]. We obtained the optimized structures of  $\text{Cp}_2\text{MCl}_2$  ( $\text{Cp} = \pi\text{-C}_5\text{H}_5$ ,  $\text{M} = \text{Ti, Zr, Hf}$ ) by density functional method with B3LYP and PW91XC as the exchange and correlation functionals, respectively. Fig. 1 shows the sketch of the optimized structure. Our results indicated that these complexes were iso-structural series with a bent sandwich. Slightly different from the literature work [11,12], this calculation did not show any symmetry that arose from the intersection of two Cp five rings. The optimized structures calculated by the present methods were more stable than those when using  $C_2$  symmetry. For instance, the total energy was  $-140.98$  eV at the present geometry, while it is  $-136.07$  eV at  $C_2$  symmetry for  $\text{Cp}_2\text{TiCl}_2$ . Table 1 lists the data of optimized geometries of the complexes along with the results by electronic diffraction. It can be seen that by PW91XC functionals, the bond lengths of M–Cl and the average distance between the metals to the centers of cyclopentadienyl (M–Cp) were 2.35 and 2.05 Å for  $\text{Cp}_2\text{TiCl}_2$ , 2.45 and 2.26 Å for  $\text{Cp}_2\text{ZrCl}_2$ , respectively, which were much closer to the experimental values (2.36 and 2.06 Å for  $\text{Cp}_2\text{TiCl}_2$ , 2.44 and 2.26 Å for  $\text{Cp}_2\text{ZrCl}_2$ ). Similar results have been obtained by using B3LYP functionals. It is clear that our calculations have reproduced the geometrical structures of these triad complexes. With increasing ionic size from Ti, Zr, to Hf, the bond lengths of M–Cl and the distance of M–Cp are expected to increase. However, our calculation gave a small decrease in the bond length of M–Cl and M–Cp from zirconocene to hafnocene, which can be explained by the effect of lanthanide contraction. On the other hand, the M–Cl bond lengths of  $\text{Cp}_2\text{MCl}_2$  ( $\text{M} = \text{Ti, Zr, Hf}$ ) in Table 1 were all longer than those for the tetrahedral complexes  $\text{TiCl}_4$  (2.17 Å),  $\text{ZrCl}_4$  (2.32 Å), and  $\text{HfCl}_4$  (2.34 Å) that do not contain cyclopentadienyl

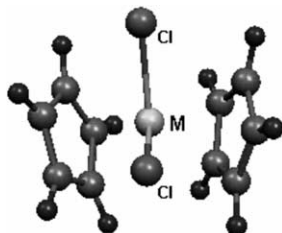


Fig. 1. Optimized structure of the complex  $\text{Cp}_2\text{MCl}_2$ .

ligands. Therefore,  $\pi$ -bonded cyclopentadienyl rings are believed to be the main reason for weakening the metal–halide bonds owing to the electronic transfer and steric hindrance.

The optimized structures of the first lowest lying triplet state for these complexes were calculated by these methods. The wave function and related properties of the triplet states can be obtained by setting up the value of spin equal to two. The wavefunction obtained by this way should be the eigenfunction of the square of the total spin angular momentum ( $S^2$ ) [24]. The results in Table 1 indicated that by using PW91XC functional, the distance of M–Cp was nearly constant in the transition process from ground state to excited state. However, the bond lengths of M–Cl were different at ground state and excited state. Similar results have been achieved by B3LYP functional with the exception that the optimized geometry of  $\text{Cp}_2\text{ZrCl}_2$  has not been obtained because no convergence result can be reached. The  $S^2$  expectation values of the triplet state by B3LYP are 2.008 and 2.004 for titanocene and hafnocene, respectively (see Table 1), giving an indication of a negligible spin contamination. Therefore, the geometries and related properties of triplet state calculated by the present methods are reliable. The change in bond lengths is known to be associated with the overlap populations of corresponding bonds. The larger bond overlap populations would represent the stronger bond strengths. Fig. 2 shows the overlap populations for  $\text{Cp}_2\text{MCl}_2$  ( $\text{Cp} = \pi\text{-C}_5\text{H}_5$ ,  $\text{M} = \text{Ti, Zr, Hf}$ ) in ground state and excited state. It can be seen that the overlap populations of M–Cp were small and did not show any striking change with the transition from ground state to excited state. But for the M–Cl bond, the overlap populations were much bigger compared with those of M–Cp, and the value was dramatically increased with the transition from ground state to excited state. These results demonstrated that with the transition from ground state to excited state, the bond strengths of M–Cl were weakened. This is in agreement with the variations of the corresponding bond lengths.

The compositions calculated for some selective orbitals are given in Table 2. The HOMO-1 represents the lower energy orbital that is nearest to the highest occupied molecular orbital (HOMO) orbital, while LUMO+1 is the higher energy orbital that is adjacent to the lowest unoccupied molecular orbital (LUMO) orbital. The sets of HOMOs had the mixed compositions from cyclopentadienyl and halide ligands, but the fraction of the compositions for each ligand was different in these orbitals. For HOMO orbitals of  $\text{Cp}_2\text{MCl}_2$  ( $\text{M} = \text{Ti, Zr, Hf}$ ), the fraction of composition for  $\pi$ -cyclopentadienyl was about 40.7% for titanocene, 51.0% for zirconocene, and 58.6% for hafnocene, while that for chloride ligands was about 42.2, 30.7 and 29.4%, respectively. The contributions from the halide orbitals to the HOMO of the target molecules decreased from

Table 1  
Geometry structures of  $\text{Cp}_2\text{MCl}_2$  (M = Ti, Zr, Hf)

		$\text{Cp}_2\text{TiCl}_2$		$\text{Cp}_2\text{ZrCl}_2$		$\text{Cp}_2\text{HfCl}_2$	
		G	$E(T)$	G	$E(T)$	G	$E(T)$
M–Cl	PW91	2.349	2.406	2.453	2.527	2.420	2.481
	B3lyp	2.375	2.426	2.491		2.464	2.520
	Expt. <sup>a</sup>	2.364		2.440			
M–Cp	PW91	2.094	2.104	2.258	2.256	2.216	2.212
	B3lyp	2.107	2.160	2.269		2.241	2.240
	Expt. <sup>a</sup>	2.059		2.260			
C–C	PW91	1.419	1.423	1.420	1.428	1.420	1.428
	B3lyp	1.432	1.436	1.437		1.433	1.444
	Expt. <sup>a</sup>	1.380		1.420			
C–H	PW91	1.084	1.084	1.084	1.085	1.084	1.084
	B3lyp	1.079	1.080	1.081		1.081	1.080
	Expt. <sup>a</sup>	1.080		1.081			
Cp–M–Cp	PW91	131.7	129.5	129.9	128.0	129.8	127.3
	B3lyp	132.2	132.1	129.7		129.9	129.8
	Expt. <sup>a</sup>	131		126.7			
$S^2$			2.008				2.004

G denotes ground state and  $E(T)$  the triplet state.

<sup>a</sup> Experimental values come from Refs. [18,19].

titanocene, zirconocene, and to hafnocene. In contrast, the contributions from the  $\pi$ -cyclopentadienyl to HOMO increased, which means the interaction between cyclopentadienyl and metals increased. This is consistent with the assignments and the tendency of the first cyclopentadienyl ionization energies by UV photoelectron spectroscopy [25,37]. The sets of LUMOs consisted primarily of the d orbitals of the central metals. The composition of the metal in the LUMO orbital was 73.8% for titanocene, 53.4% for zirconocene, and 54.3% for hafnocene, respectively. However, the compositions of the cyclopentadienyl showed a systematic increase such as from 4% for titanocene, 13.9% for zirconocene, to 22.3% for hafnocene. The energy levels of these

frontier molecular orbitals are given in Fig. 3. The HOMOs of  $\text{Cp}_2\text{MCl}_2$  (M = Ti, Zr, Hf) had a nearly constant energy level since these orbitals consisted mainly of the same ligands. The LUMOs showed a big shift to higher energy in going from  $\text{Cp}_2\text{TiCl}_2$ ,  $\text{Cp}_2\text{ZrCl}_2$ , and to  $\text{Cp}_2\text{HfCl}_2$ , which can be explained by the increase of d orbital energies of the central metals from Ti, Zr, to Hf. Therefore it can be concluded that the low-lying excitations were the excitations of the electron from the  $\pi$ -type orbitals of ligands in HOMOs to the d orbitals of the central metals in LUMOs.

HIRSHEFLD analysis can produce the charge value per fragment in molecule, and atomic charge values if each atom is used as fragment. The values of HIR-SHEFLD charges are computed as the integral of the SCF charge density over space, in each point weighted by the relative fraction of the (initial) density of that fragment in the total initial (sum-of-fragments) density [38]. These values are used to represent the relative distribution of electrons in complexes. The HIR-SHEFLD charges for both ground and excited state of  $\text{Cp}_2\text{MCl}_2$  (Cp =  $\pi$ -C<sub>5</sub>H<sub>5</sub>, M = Ti, Zr, Hf) are listed in Table 3. From the HIR-SHEFLD charges, it is seen that during the transition from ground state to excited state, the central metals accepted certain electrons by decreasing the charge from 0.345 to 0.252 for titanocene, 0.503 to 0.368 for zirconocene, and 0.539 to 0.419 for hafnocene. These accepted electrons came primarily from the ligands of Cp. This electronic transfer led to an increase in the charge of Cp ligands. The charges of Cl ligands were barely influenced by the transition from ground state to excited state, even though the contribu-

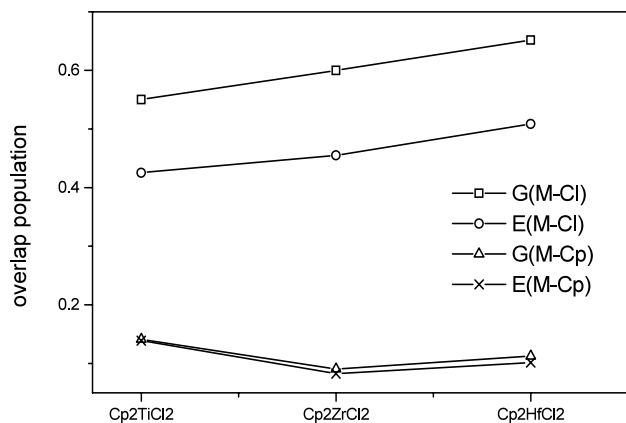


Fig. 2. Overlap populations of M–Cl and M–Cp bonds at ground (G) state and excited state (E) for the complexes  $\text{Cp}_2\text{MCl}_2$  (M = Ti, Zr, Hf).

Table 2  
Composition of several selected orbitals for  $Cp_2MCl_2$  (M = Ti, Zr, Hf)

	HOMO-2	HOMO-1	HOMO	LUMO	LUMO+1	LUMO+2
<i>Cp<sub>2</sub>TiCl<sub>2</sub></i>						
Ti	1.77	5.18	5.26	73.82	71.21	56.15
Cl	67.70	57.92	42.23	15.83	2	16.77
Cp	21.12	27.08	40.71	4.02	17.04	14.40
<i>Cp<sub>2</sub>ZrCl<sub>2</sub></i>						
Zr	1.93	4.93	2.24	53.42	44.02	69.65
Cl	41.19	48.23	30.72	13.81	10.53	3.23
Cp	47.58	37.11	50.96	13.93	44.17	23.94
<i>Cp<sub>2</sub>HfCl<sub>2</sub></i>						
Hf	1.85	5.00	1.97	54.31	32.12	58.90
Cl	43.91	46.13	29.43	12.48	7.84	2.72
Cp	42.47	39.86	58.59	22.28	58.72	34.36

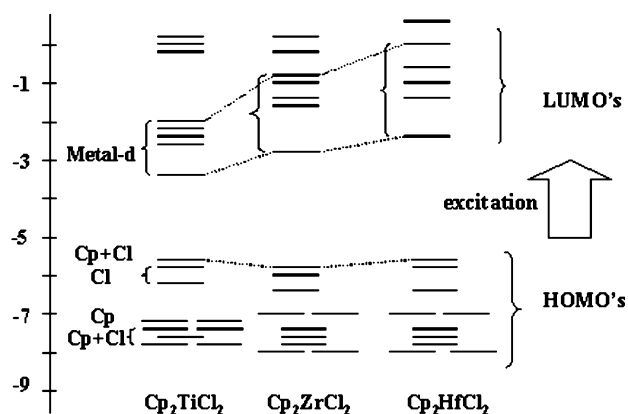


Fig. 3. Energy levels of several selected molecular orbitals for  $Cp_2TiCl_2$ ,  $Cp_2ZrCl_2$ , and  $Cp_2HfCl_2$ .

tion of Cl ligands to HOMO orbital was comparable to that of Cp ligands (see Table 2). Fig. 4 illustrates the difference of charges between ground state and excited state for the central metals and ligands. The charge variations for Cl ligands were nearly zero in these complexes. The values of charge decrease for the ligands Cp were approximately equal to the values of charge increase for the central metals. These results showed that the electron density of the complexes was redistributed during the excitation by an electronic transfer from the

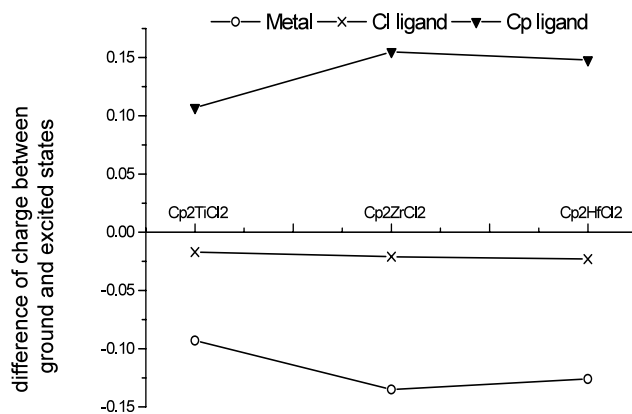


Fig. 4. Charge differences with the complexes changing from ground to excited states.

ligands Cp to the central metals. The electronic redistribution can be confirmed experimentally through the change of dipole moment between the ground- and excited-state of the complexes [39]. The electrons leave a 'donor' molecular fragment of Cp ligands, travel a macroscopic distance comparable to the fragment size, and then end up on an 'acceptor' fragment of the central metals during the transition. This kind of charge transfer results in certain displacement of the electron density. The change of dipole moment between ground

Table 3  
HIRSHEFLD charges in the ground state and excited state for  $Cp_2MCl_2$  (M = Ti, Zr, Hf)

	$Cp_2TiCl_2$		$Cp_2ZrCl_2$		$Cp_2HfCl_2$	
	G	<i>E</i> (T)	G	<i>E</i> (T)	G	<i>E</i> (T)
M	0.3449	0.2520	0.503	0.3679	0.5391	0.4128
Cl	-0.2029	-0.2119	-0.2275	-0.2365	-0.2243	-0.2355
Cl	-0.2041	-0.2119	-0.2249	-0.2373	-0.2240	-0.2365
Cp1	0.0326	0.0868	-0.0248	0.0616	-0.0463	0.0410
Cp2	0.0346	0.0873	-0.0216	0.0464	-0.0405	0.0201

G donates ground state and *E*(T) triplet state.

state and excited state is determined by the extent of this charge redistribution. The dipole moments of the complexes  $\text{Cp}_2\text{MCl}_2$  ( $\text{M} = \text{Ti}, \text{Zr}, \text{Hf}$ ) calculated by our methods are listed in Table 4. The dipole moments decreased slightly from titanocene, zirconocene, to hafnocene. This can be explained by the different distribution of electrons. From Table 3, it is seen that the charges of Cp ligands became more negative from  $\text{Cp}_2\text{TiCl}_2$ ,  $\text{Cp}_2\text{ZrCl}_2$ , and to  $\text{Cp}_2\text{HfCl}_2$ . Therefore, the dipole moments of M–Cl bonds were partially cancelled by the M–Cp bond dipole moments, yielding a decrease in dipole moments from  $\text{Cp}_2\text{TiCl}_2$ ,  $\text{Cp}_2\text{ZrCl}_2$ , and to  $\text{Cp}_2\text{HfCl}_2$ . With the transition from the ground state to excited state, the charge transfer from Cp ligands to central metal would give a larger displacement of electron density, even though the variation of geometry structure is appreciably small. Therefore, a shift of the center of the positive charge toward the Cp ligands is expected with the change from ground state to excited state, which would increase the distance between the centers of the positive and negative charges. As a consequence, the dipole moments in the excited state were increased. From the above results, it can be concluded that the LMCT transitions were associated with a shift of electron density from the ligands Cp to the central metals.

### 3.2. Assignments of electronic spectra

The electronic absorption spectra of the complexes  $\text{Cp}_2\text{MCl}_2$  ( $\text{Cp} = \pi\text{-C}_5\text{H}_5$ ,  $\text{M} = \text{Ti}, \text{Zr}, \text{Hf}$ ) exhibit a first weak band and a stronger band at a sequence of energy in near UV–vis region [20]. The energies of the low-lying absorption bands become stronger from titanocene, zirconocene, and to hafnocene, showing a strong dependence on the central metals. In this work, the electronic spectra are revisited theoretically by the TDDFT method. Tables 5 and 6 summarize the vertical excitation energies and oscillator strengths for the spin-allowed excited states calculated by the method of TDDFT with the correction and exchange functionals of B3LYP for GAUSSIAN-98 code (TDDFT-B3LYP) and PW91XC for ADF1999 code (TDDFT-PW91XC). These two different methods have produced similar results of excitation energies for these triad complexes.

Table 4  
Dipole moments of the ground state and excited state for  $\text{Cp}_2\text{MCl}_2$  ( $\text{M} = \text{Ti}, \text{Zr}, \text{Hf}$ )

	$\text{Cp}_2\text{TiCl}_2$	$\text{Cp}_2\text{ZrCl}_2$	$\text{Cp}_2\text{HfCl}_2$
D-ground state	4.6930	4.3573	4.2923
D-triplet	5.7838	5.8826	5.6866
$\Delta\text{D}^*$	1.0908	1.5256	1.3943

\*Denotes the difference of dipole moment between ground state and excited state.

Table 5  
Vertical excitation energies and oscillator strengths of singlet–singlet excitations by the method of TDDFT-PW91XC for  $\text{Cp}_2\text{MCl}_2$  ( $\text{M} = \text{Ti}, \text{Zr}, \text{Hf}$ )

	$\text{Cp}_2\text{TiCl}_2$		$\text{Cp}_2\text{ZrCl}_2$		$\text{Cp}_2\text{HfCl}_2$	
	Ev	Os	Ev	Os	Ev	Os
1	2.26	0.0011	3.28	0.0049	3.57	0.0061
2	2.48	0.0000	3.50	0.0002	3.82	0.0003
3	2.96	0.0250	3.83	0.0336	4.20	0.0433
4	3.33	0.0047	4.36	0.0000	4.61	0.0001
5	3.36	0.0021	4.42	0.0004	4.79	0.0019
6	3.39	0.0004	4.53	0.0098	4.82	0.0192
7	3.52	0.0110	4.54	0.0101	4.95	0.0012
8	3.55	0.0033	4.57	0.0046	5.01	0.0205
9	3.66	0.0002	4.69	0.0024	5.07	0.0000
10	3.69	0.0165	4.76	0.0002	5.16	0.0021

Table 6  
Vertical excitation energies and oscillator strengths of singlet–singlet excitations by the method of TDDFT-B3LYP for  $\text{Cp}_2\text{MCl}_2$  ( $\text{M} = \text{Ti}, \text{Zr}, \text{Hf}$ )

	$\text{Cp}_2\text{TiCl}_2$		$\text{Cp}_2\text{ZrCl}_2$		$\text{Cp}_2\text{HfCl}_2$	
	Ev	Os	Ev	Os	Ev	Os
1	2.35	0.0001	3.41	0.0006	3.86	0.0010
2	2.59	0.0000	3.64	0.0000	4.14	0.0001
3	3.03	0.0020	3.93	0.0044	4.48	0.0071
4	3.29	0.0000	4.42	0.0000	5.06	0.0000
5	3.33	0.0005	4.51	0.0001	5.13	0.0000
6	3.34	0.0001	4.65	0.0029	5.29	0.0053
7	3.50	0.0010	4.69	0.0006	5.33	0.0013
8	3.58	0.0005	4.74	0.0012	5.37	0.0027
9	3.65	0.0031	4.80	0.0003	5.52	0.0006
10	3.68	0.0004	4.86	0.0000	5.57	0.0004

The only difference is that the results by TDDFT-PW91XC showed a slightly underestimated energies in comparison with those by the method of TDDFT-B3LYP, e.g. the vertical excitation energy of the first relatively strong excitation was 2.26 eV for  $\text{Cp}_2\text{TiCl}_2$ , 3.28 eV for  $\text{Cp}_2\text{ZrCl}_2$ , and 3.57 eV for  $\text{Cp}_2\text{HfCl}_2$  by the method of TDDFT-PW91XC, while by the method of TDDFT-B3LYP, this excitation energy was 2.35, 3.41 and 3.86 eV, respectively. These results are consistent with the experimental data in Tables 5 and 6. It is also seen that the method of TDDFT-B3LYP with a hybrid functional of HF and DFT could produce more accurate results than those by the method of TDDFT-PW91XC for these complexes. In order to understand the effect of different functionals, the transition energies of the first 16 excitations for these complexes calculated by TDDFT-PW91XC and TDDFT-B3LYP are showed in Fig. 5. For  $\text{Cp}_2\text{TiCl}_2$ , the energy of each excitation was very similar. However the difference of excitation energies by two methods became larger from  $\text{Cp}_2\text{TiCl}_2$ ,

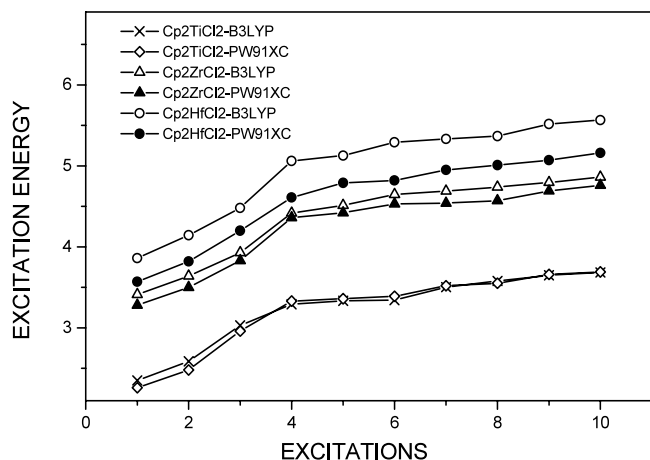


Fig. 5. Vertical excitation energies of the first 16 excitations for  $\text{Cp}_2\text{MCl}_2$  ( $M = \text{Ti}, \text{Zr}, \text{Hf}$ ).

$\text{Cp}_2\text{ZrCl}_2$ , and to  $\text{Cp}_2\text{HfCl}_2$ . This energy difference is believed to be from the approximation involving the relativistic effect. For TDDFT-PW91XC of ADF code, the relativistic effect was calibrated by applying ZORA methods, while for the methods of TDDFT-B3LYP of GAUSSIAN-98 code it was modified by setting basic sets of LANL2DZ. The calibration magnitudes of relativistic effect were therefore different for these methods, since the relativistic effect is increased from Ti, Zr, to Hf.

On the other hand, the oscillator strengths obtained by these two methods showed a similar trend, e.g., by varying the central metals, they showed a pronounced increase from 0.0011 for titanocene, 0.0049 for zirconocene, and 0.0061 for hafnocene by the method of TDDFT-PW91XC. Similarly, by the method of TDDFT-B3LYP, the relative oscillator strengths were increased from 0.0001 for titanocene, 0.0006 for zirconocene, and to 0.0010 for hafnocene, respectively. The variations of oscillator strength can be understood in terms of the increased fracture of the composition of Cp ligand at sets of higher occupied orbitals from titanocene, zirconocene, and hafnocene, since the lower MLCT excitation was originated from Cp to the central metals. This trend exactly follows the molar absorptivity observed experimentally [20]. The oscillator strengths of the second relatively strong excitation were considerably larger than those of the first excitations, which matched well the relative intensity measured experimentally [20]. Therefore, the present calculations have accurately described the electronic spectra of the group IV metallocene triad.

We also performed the calculations using the method of  $\Delta\text{SCF-DFT}$  by the Ziegler's sum mechanism to get the excitation energies at lowest lying excited states. For  $\Delta\text{SCF}$  method of ADF program, the energy of Frank-Condon excitation in the singlet state is obtained by fixing the electrons at the corresponding orbital with opposite spin directions in order to simulate the desired

electronic states. The state obtained by this method is not a really singlet state but a mixed state of singlet and corresponding triplet [24]. The energies for the triplet and mixed states are individually calculated using the density functional methods. The energies of the singlet was thus given by the formula of  $E(\text{singlet}) = 2E(\text{mixed}) - E(\text{triplet})$ . These results are listed in Table 7 along with the results obtained by other methods. The experimental data are also given for comparison. It is clear that the results of  $\Delta\text{SCF-DFT}$  have produced reliable vertical excitation energies comparable with the experimental values. However, the numbers of the states that can be obtained by this method are only limited to several lowest excited states because of the convergence problem. For the higher excited states, it is difficult to get optimized structure using  $\Delta\text{SCF-DFT}$  method.

The properties of adsorption band can be well explained on the base of our calculation. The first absorption band was assigned to the first and second excitations. The first excitation corresponds to the electron transfer from HOMO to LUMO orbital. From Fig. 6, it is seen that the HOMO orbitals were nonbonding orbital of Cp and Cl ligands, while the LUMO orbital consisted of the  $dx^2 - y^2$  orbital of the central metals and a  $\pi$ -type orbitals of the Cl ligands. It is known that the electronic transfer in this excitation is mainly from Cp ligands to central metals. This excitation process is expected to enlarge the M-Cl bond length by increasing the repulsive interaction between the central metals and Cl ligands. This is consistent with the results of optimized structures of both ground state and excited state. The second excitation involving the electronic transfer from HOMO-1 to LUMO orbital is very similar to the first excitation with the exception that it is  $d_{xy}$  orbital of metal in HOMO and  $d_{yx}$  orbital in HOMO-1, respectively (see Fig. 6). The third excitation from HOMO-2 to LUMO, having similar characteristics to the first and second excitations, is the strongest excitation, and has been assigned to the second adsorption band that is becoming broader owing to the contribution of the fourth excitation with a slightly weaker oscillator strength (see Fig. 7). The fourth excitation corresponded to an electronic transfer from HOMO to LUMO+2 that has an orbital characteristic involving  $\sigma$  repulsive interaction between the central metals and Cl ligands. The fifth excitation was from HOMO-3 to LUMO, and the HOMO-3 orbital was made up of the strong bonding orbital between the metals and Cp ligands. The fifth excitation shifted to the higher energy in order to overcome the higher bonding energy between M and Cp ligands (Fig. 7). It can be concluded from our analysis that the first and second adsorption bands were all from the electronic transfer from the ligands to the central metals.

The complexes  $\text{Cp}_2\text{MCl}_2$  ( $\text{Cp} = \pi\text{-C}_5\text{H}_5$ ,  $M = \text{Ti}, \text{Zr}, \text{Hf}$ ) exhibit an intense, long-lived charge transfer phos-

Table 7

Comparison of the vertical excitation energies for the singlet states by different methods for  $Cp_2MCl_2$  ( $M = Ti, Zr, Hf$ )

	TDDFT-Pw91xc	TDDFT-B3lyp	$\Delta$ SCF-DFT	SCF-X $\alpha$ -SW[26]	CNDO[25]	Expt.[20]
$Cp_2TiCl_2$						
First	2.26	2.35	2.32	1.7	3.03	2.4
Second	2.96	3.03		2.1	3.88	3.2
$Cp_2ZrCl_2$						
First	3.28	3.41	3.30			3.73
Second	3.83	3.93				4.28
$Cp_2HfCl_2$						
First	3.57	3.86				4.04
Second	4.20	4.48				4.76

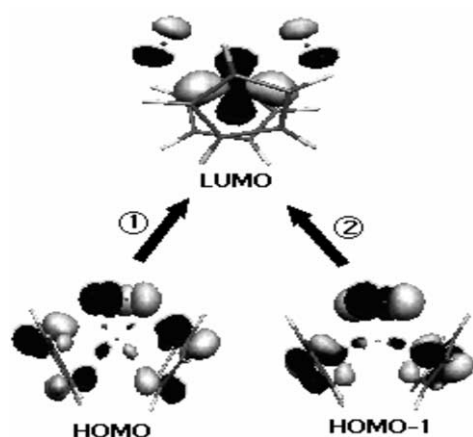


Fig. 6. Counter plot of the molecular orbitals related to the first and second excitations.

phorescence emission at 77 K [20]. For all these complexes, the emissive lifetimes are as long as 800, 2000 and 300  $\mu$ s, and the emitting energies are shifted to the higher energy level from  $Cp_2TiCl_2$ ,  $Cp_2ZrCl_2$ , and to

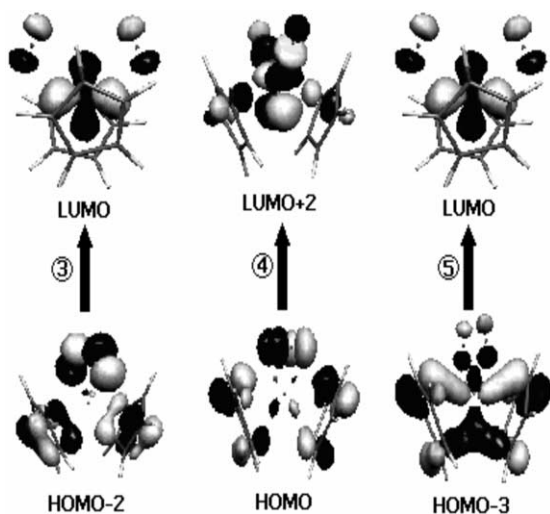


Fig. 7. Counter plot of the molecular orbitals related to the third, fourth, and fifth excitations.

$Cp_2HfCl_2$ . The difference in radiation lifetimes and the emitting energies indicated that the phosphorescence relaxation process is dramatically affected by the nature of the metal–ligand  $\pi$ -bonding. With regards to the relationship between phosphorescence emission and the properties of triplet excited states, we also studied the excitation of singlet to triplet by TDDFT method. The calculations were performed using the optimized structure of ground state by a response module in ADF. The results are summarized in Tables 8 and 9. The energy of the first excitation of  $Cp_2MCl_2$  ( $M = Ti, Zr, Hf$ ) was 2.13, 3.13 and 3.39 eV by the method of TDDFT-PW91XC, and 2.16, 3.20 and 3.61 eV by the method of TDDFT-B3LYP. These values are in excellent agreement with the energies of 2.08, 3.01 and 3.26 eV for the 0–0 excitation at first emission band as determined from the phosphorescence spectra of the three complexes. The excitation energies shifted to the higher energy level with varying the central metals from titanocene, zirconocene, and to hafnocene. Because the phosphorescence occurs as the electron transfer from the triplet state to the stable state, the transition energy is dependent on the gaps between LUMOs and HOMOs. Therefore, the excitation energies become larger with the increased gap of HOMOs-to-LUMOs from titanocene, zirconocene, and to hafnocene. A comparison has been done for the

Table 8

Vertical excitation energies of singlet–triplet excitations by the method of TDDFT-PW91XC for  $Cp_2MCl_2$  ( $M = Ti, Zr, Hf$ )

Excitation	$Cp_2TiCl_2$	$Cp_2ZrCl_2$	$Cp_2HfCl_2$
1	2.13	3.13	3.39
2	2.34	3.34	3.63
3	2.55	3.48	3.80
4	3.01	4.11	4.30
5	3.19	4.21	4.54
6	3.28	4.23	4.56
7	3.37	4.25	4.59
8	3.38	4.33	4.69
9	3.42	4.48	4.76
10	3.44	4.50	4.97

Table 9  
Vertical excitation energies of singlet–triplet excitation by the method of TDDFT-B3LYP for  $\text{Cp}_2\text{MCl}_2$  (M = Ti, Zr, Hf)

Excitation	$\text{Cp}_2\text{TiCl}_2$	$\text{Cp}_2\text{ZrCl}_2$	$\text{Cp}_2\text{HfCl}_2$
1	2.16	3.20	3.61
2	2.40	3.43	3.87
3	2.61	3.54	3.99
4	2.69	4.08	4.56
5	3.03	4.17	4.65
6	3.04	4.26	4.83
7	3.14	4.28	4.88
8	3.14	4.35	4.93
9	3.26	4.40	5.08
10	3.38	4.47	5.12

excitation energies of lower lying triplet states obtained by different methods (Table 10). The methods of TDDFT have been proved to produce good results as expected. The reliable results for these complexes have also been obtained by the method of  $\Delta\text{SCF-PW91XC}$ . However  $\Delta\text{SCF-B3LYP}$  method underestimated the magnitudes compared with those by other methods for  $\text{Cp}_2\text{TiCl}_2$ , while the value of 3.22 for  $\text{Cp}_2\text{HfCl}_2$  seems to well fit the experiment data. This is because we have taken into account the underestimation by the method of  $\Delta\text{SCF-B3LYP}$  and overestimation due to a large relativistic effect.

#### 4. Conclusions

This work investigated the excitation of the LMCT in the UV–vis spectra of the complexes  $\text{Cp}_2\text{MCl}_2$  ( $\text{Cp} = \pi\text{-C}_5\text{H}_5$ , M = Ti, Zr, Hf) by density functional theory. The nature of the main spectral features has been interpreted on the basis of the electronic structure of the complexes. These complexes represented an iso-structural series with a pseudotetrahedral geometry. The bond length of M–Cl and the distance of M–Cp increased from M = Ti, Zr, and Hf. Both  $\text{Cp}_2\text{ZrCl}_2$  and  $\text{Cp}_2\text{HfCl}_2$  exhibited analogous electronic structure and properties owing to the effects of lanthanide contraction. With the

Table 10  
Comparison of the vertical excitation energies for the triplet state by different methods for  $\text{Cp}_2\text{MCl}_2$  (M = Ti, Zr, Hf)

	$\text{Cp}_2\text{TiCl}_2$	$\text{Cp}_2\text{ZrCl}_2$	$\text{Cp}_2\text{HfCl}_2$
TDDFT-PW91XC	2.13	3.13	3.39
TDDFT-B3LYP	2.16	3.20	3.61
$\Delta\text{SCF-PW91XC}$	2.10	2.94	3.11
$\Delta\text{SCF-B3LYP}$	1.59		3.22
Expt. (0–0)[20]	2.08	3.08	3.24

transition from ground state to excited state, the electron transferred from Cp ligands to the central metals, accompanying with an increase in the bond length of M–Cl. The two lowest adsorption bands for these complexes are predominantly corresponding to the excitation of charge transfer from Cp ligand to the metals in character. The energies and oscillator strengths of the lowest excitations depended strongly on the central metals. The LUMOs of mainly metallic d orbital increased in energy from titanocene, zirconocene, and to hafnocene. The HOMOs of primarily Cp and Cl ligands in character were relatively stable. The overall effect was thus to increase the energy gap between the HOMOs and the LUMOs so as to increase the excitation energies along this series. The increase in oscillator strengths is due to the increase in the fraction of Cp composition at LUMOs from titanocene, zirconocene, and to hafnocene under the assumption that the LMCT excitation is originated from the electronic transfer from Cp to the central metals. The results of triplet states have been used to simulate the phosphorescence spectrum. The predicted level patterns of the lowest triplet excited states are in excellent agreement well with the phosphorescence data available.

#### References

- [1] V. Balzani, *Supramolecular Photochemistry*, Reidel, Dordrecht, Holland, 1987.
- [2] G.L. Geoffroy, M.S. Wrighton, *Organometallic Photochemistry*, Academic Press, New York, 1979.
- [3] D.M. Roundhill, *Photochemistry and Photophysics of Metal Complexes*, Academic Press, New York, 1994.
- [4] R.F. Jordan, *Adv. Organomet. Chem.* 32 (1991) 325.
- [5] D.V. Scaltrito, D.W. Thompson, J.A. O'Callaghan, G.J. Meyer, *Coord. Chem. Rev.* 208 (2000) 243.
- [6] (a) A. Vogler, H. Kunkely, *Coord. Chem. Rev.* 177 (1998) 81; (b) H. Kunkely, A. Vogler, *J. Am. Chem. Soc.* 117 (1995) 540.
- [7] B.D. Rossenaar, D.J. Stufkens, A. Vlcek, Jr., *Inorg. Chim. Acta* 35 (1996) 2902.
- [8] I.R. Farrell, A. Vlcek, Jr., *Coord. Chem. Rev.* 208 (2000) 87.
- [9] (a) J.W. Kenney, III, D.R. Boone, D.R. Striplin, Y.-H. Chen, K.B. Hamar, *Organometallics* 12 (1993) 3671; (b) M.R.M. Bruce, D.R. Tyler, *Organometallics* 4 (1985) 528.
- [10] G. Wilkinson, J.M. Birmingham, *J. Am. Chem. Soc.* 76 (1954) 4281.
- [11] A. Clearfield, D.K. Warner, C.H. Daldarriaga-Molina, R. Ropal, I. Bernal, *Can. J. Chem.* 53 (1975) 1622.
- [12] (a) P. Keith, T.S. Cameron, F.A. Roger, C.R. Stephen, D. Barry, R.V. Graham, *Acta Crystallogr. B* 30 (1974) 2290; (b) J.L. Atwood, W.E. Hunter, D.C. Hrcncir, E. Samuel, H. Alt, M.D. Rausch, *Inorg. Chem.* 14 (1975) 1757.
- [13] V.V. Strelets, *Coord. Chem. Rev.* 114 (1992) 1.
- [14] G.V. Loukova, O.N. Babkina, T.A. Bazhenova, N.M. Bravaya, V.V. Strelets, *Izv. Acad. Nauk. Ser. Khim.* 49 (2000) 60.
- [15] G.V. Loukova, V.V. Strelets, *J. Organomet. Chem.* 606 (2000) 203.
- [16] N.A. Beach, H.B. Gray, *J. Am. Chem. Soc.* 90 (1968) 5713.
- [17] A. Vogler, H. Kunkely, *Coord. Chem. Rev.* 177 (1998) 81.

- [18] V.W.W. Yam, G.Z. Qi, K.K. Cheung, *J. Chem. Soc. Dalton Trans.* (1998) 1819.
- [19] V.W.W. Yam, G.Z. Qi, K.-K. Cheung, *Organometallics* 17 (1998) 5448.
- [20] G.V. Loukova, V.A. Smirnov, *Chem. Phys. Lett.* 329 (2000) 437.
- [21] (a) J.L. Petersen, D.L. Lichtenberger, R.F. Fenske, L.F. Dahl, *J. Am. Chem. Soc.* 97 (1975) 6433;  
(b) J.W. Lauher, R.J. Hoffmann, *Am. Chem. Soc.* 98 (1976) 1729.
- [22] (a) H. Arne, V.V. Hans, O. Kari-Anne, M. Miguel, Y. Carlos, P. Federico, *J. Mol. Struct.* 567–568 (2001) 295;  
(b) J.G. Lee, H.Y. Jeong, Y.H. Ko, J.H. Jang, H. Lee, *J. Am. Chem. Soc.* 122 (2000) 6476.
- [23] (a) R. Fusco, L. Longo, F. Masi, F. Garbassi, *Macromolecules* 30 (1997) 7673;  
(b) M.L. Ferreira, D.E. Damiani, A. Juan, *Comput. Mater. Sci.* 9 (1998) 357.
- [24] H. Jurg, M. Dominik, P.J. Michele, *Chem. Phys.* 108 (1998) 4060.
- [25] G. Condorelli, I. Fragala, A. Centineo, E. Tondello, *J. Organomet. Chem.* 87 (1975) 311.
- [26] M.R.M. Bruce, A. Kenter, D. Tyler, *J. Am. Chem. Soc.* 106 (1984) 639.
- [27] W.C. Ermler, Y.S. Lee, K.S. Pitzer, *J. Chem. Phys.* 70 (1979) 293.
- [28] F.C. Guerra, J.G. Snijders, B. Velde, E.J. Baerends, *Theor. Chem. Acc.* 99 (1998) 391.
- [29] A.D. Becke, *J. Chem. Phys.* 98 (1993) 5648.
- [30] P.J. Hay, W.R. Wadt, *J. Chem. Phys.* 82 (1985) 270, 284, 299.
- [31] J.P. Perdew, J.A. Chevary, S.H. Vosko, K.A. Jackson, M.R. Pederson, D.J. Singh, *Phys. Rev. A* 46 (1992) 6671.
- [32] E.V. Lenth, A.E. Ehlers, E.J. Baerends, *J. Chem. Phys.* 110 (1999) 8943.
- [33] E.K.U. Gross, J.F. Dobson, M. Petersilka, *Density Functional Theory of Time-Dependent Phenomena*, Springer, New York, Heidelberg, 1996.
- [34] M.E. Casida, in: J.M. Seminario (Ed.), *Time-Dependent Density Functional Response Theory of Molecular System: Theory, Computational Methods, and Functionals in Recent Developments and Applications of Modern Density Functional Theory*, Elsevier, Amsterdam, 1996.
- [35] T. Ziegler, A. Rauk, E.J. Baerends, *Theor. Chim. Acta* 43 (1977) 261.
- [36] S. Portmann, H.P. Luthi, *Chimia* 54 (2000) 766.
- [37] (a) Z.T. Tsai, C.H. Brubaker, Jr., *J. Organomet. Chem.* 166 (1979) 199;  
(b) M.R.M. Bruce, A. Sclafani, D.R. Tyler, *Inorg. Chem.* 25 (1986) 2546.
- [38] F.L. Hirschfeld, *Theor. Chim. Acta* 44 (1977) 129.
- [39] N.S. Hush, J.R. Reimers, *Coord. Chem. Rev.* 177 (1998) 37.